Chemical Science

ROYAL SOCIETY OF CHEMISTRY

REVIEW

View Article Online
View Journal | View Issue



Cite this: *Chem. Sci.*, 2022, **13**, 7378

# State-of-the-art accounts of hyperpolarized $^{15}$N-labeled molecular imaging probes for magnetic resonance spectroscopy and imaging

Hyejin Park and Qiu Wang *

Hyperpolarized isotope-labeled agents have significantly advanced nuclear magnetic resonance spectroscopy and imaging (MRS/MRI) of physicochemical activities at molecular levels. An emerging advance in this area is exciting developments of $^{15}$N-labeled hyperpolarized MR agents to enable acquisition of highly valuable information that was previously inaccessible and expand the applications of MRS/MRI beyond commonly studied $^{13}$C nuclei. This review will present recent developments of these hyperpolarized $^{15}$N-labeled molecular imaging probes, ranging from endogenous and drug molecules, and chemical sensors, to various $^{15}$N-tagged biomolecules. Through these examples, this review will provide insights into the target selection and probe design rationale and inherent challenges of HP imaging in hopes of facilitating future developments of $^{15}$N-based biomedical imaging agents and their applications.

Received 2nd March 2022
Accepted 17th May 2022

DOI: 10.1039/d2sc01264b

rsc.li/chemical-science



## 1. Introduction

### 1.1. Magnetic resonance spectroscopy and imaging – general information and limitations

Magnetic resonance spectroscopy and imaging (MRS/MRI) are powerful non-invasive molecular imaging modalities that provide biochemical and anatomical information about the human body. MR imaging mainly concerns the generation of anatomical images translated into spatial maps to distinguish healthy tissues from diseased areas.[1] MR spectroscopy, performed along with MRI, analyzes chemical processes and metabolic contents of the scanned tissue. MRS offers qualitative and quantitative assessments of various MR-active nuclei (*i.e.*, $^{1}$H, $^{13}$C, $^{15}$N, and $^{31}$P) in metabolites using chemical shift assignments in the NMR spectra.[2,3] Therefore, MRI and MRS have been routinely used in research and clinical practices as imperative diagnostic techniques that offer valuable biochemical and anatomical information. Despite these advancements, magnetic resonance spectroscopic technologies suffer from low sensitivity and clinical MRS/MRI are restricted to the most abundant proton ($^{1}$H) resonances as the signal source.

All MR scans are evolved from nuclear magnetic resonance (NMR) and the imaging sensitivity mainly relies on the abundance and polarization levels of nuclear spins. As thermal polarization levels of nuclear spins are small, traditional $^{1}$H-MRI detects highly abundant $^{1}$H signals in the form of water and fat to provide sufficient sensitivity. Yet scanning other MR-active nuclei found in biomolecules is challenging due to their low natural abundances. For example, carbon and nitrogen are among the most common elements found in the structures of biomolecules. The natural abundance for $^{13}$C and $^{15}$N is only 1.1% and 0.37%, respectively, in comparison to 99.99% for $^{1}$H (Table 1).[4] Other factors related to the MR signal intensity are the gyromagnetic ratio ($\gamma$) and concentration of the nuclei of interest. The $\gamma$ value directly correlates with the NMR signal sensitivity; for instance, $^{13}$C has a low gyromagnetic ratio, which is less than 1/4 of $\gamma(^{1}\mathrm{H})$, and therefore has a lower relative sensitivity to $^{1}$H. Furthermore, the ultra-low $\gamma$ of $^{15}$N (1/10 of $\gamma(^{1}\mathrm{H})$) translates into a significant decrease in sensitivity.

In addition to the low $\gamma$ values, the sensitivity of isotope-enriched metabolites may suffer from the low concentration (sub-millimolar) of the interrogated metabolic species *in vivo*.[5] Accordingly, it is challenging to observe these isotope signals, especially those of $^{15}$N nuclei, from biomolecules *in vivo* with the conventional MRS/MRI. Yet, several hyperpolarization techniques have emerged to tackle the challenge of MR sensitivity.

### 1.2. Hyperpolarization technique and current methods

The sensitivity of MR correlates with nuclear-spin polarization. The NMR signal intensity is governed by the population difference between two nuclear spin states, also referred to as the polarization level. The polarization is affected by the gyromagnetic ratio ($\gamma$) and the magnetic field strength ($B_0$). At thermal equilibrium, polarization levels of MR-active nuclei are low (only $10^{-6}$ to $10^{-4}$), which is the reason for the low sensitivity of MRI/MRS.[6]

The hyperpolarization (HP) technique addresses the sensitivity problem and has revolutionized the field of MR

*Department of Chemistry, Duke University, Durham, NC 27708, USA. E-mail: qiu.wang@duke.edu*

Table 1 Nuclear magnetic properties of $^{1}H$, $^{13}C$ and $^{15}N$ nuclei[4]

| Nucleus | Natural abundance (%) | $\gamma$ ($10^7$ rad $T^{-1}$ $s^{-1}$) | Relative sensitivity[a] | Relative receptivity[b] |
|---|---|---|---|---|
| $^{1}H$ | 99.99 | 26.75 | 1.000 | 1.00 |
| $^{13}C$ | 1.11 | 6.73 | 0.016 | $1.70 \times 10^{-4}$ |
| $^{15}N$ | 0.37 | −2.71 | 0.001 | $3.84 \times 10^{-6}$ |

[a] At a constant magnetic field and equal number of nuclei. [b] The receptivity reflects the overall ease of acquiring an NMR signal relative to $^{1}H$ at the same magnetic field.

spectroscopy and imaging. Hyperpolarization artificially induces a nonequilibrium polarization of nuclear spins for a period of time (Fig. 1). The HP technique can enhance signal sensitivity by several orders of magnitude by increasing the spin state population difference.[6] The dramatic signal enhancements allow real-time detection of both introduced hyperpolarized imaging agents and their metabolic products. Thus, HP-MR scans of isotope-labeled probes provide unparalleled ability to monitor complex biological processes through advantageous features of the NMR spectroscopy combined with its high structural specificity, non-invasiveness, and quantitative analysis.

Among several available hyperpolarization methods, two techniques have been used mainly for polarizing non-gaseous isotopes. The first technique is dynamic nuclear polarization (DNP), which is currently the most clinically advanced method that has been used for *in vivo* hyperpolarization studies.[5,7] DNP relies on polarization transfer from electrons to the nuclei of interest dissolved in glass-forming solvents *via* microwave irradiation at low temperatures (1–2 K) for approximately 1–3 hours.[8] After polarization build-up, the frozen pellet containing a hyperpolarized imaging agent is quickly dissolved with hot water (hence dissolution-DNP, d-DNP), generating a hyperpolarized solution ready for *in vivo* imaging. d-DNP is the most established polarization method used for preclinical and clinical imaging, as according to its principle, any molecule of interest can be hyperpolarized in water.

The second hyperpolarization method uses *para*-hydrogen as the polarization transfer source.[9,10] For example, *para*-hydrogen-induced polarization (PHIP) can be achieved by catalytic hydrogenation of *para*-$H_2$ across unsaturated bonds (*e.g.*, alkene or alkyne) located near the MR-active isotope. Thus, the reduction of the unsaturated bond with a concomitant break of *para*-$H_2$ symmetry enables polarization transfer from $^{1}H$ to nearby $^{13}C$ or $^{15}N$ nuclei *via* networks of *J*-coupling.[11] The PHIP method is not generally applicable as d-DNP as the substrate needs to have an unsaturated bond. Alternatively, *para*-$H_2$ can be used to deliver polarization transfer by signal amplification by reversible exchange (SABRE) through reversible binding to a metal catalyst from both *para*-$H_2$ and the substrate.[12–14] Thus, SABRE can hyperpolarize a broader scope of substrates than the traditional PHIP method that relies on the irreversible hydrogenation reaction. The detailed mechanisms of these hyperpolarization techniques have been described in several review papers.[15–17] Overall, these developments in polarization techniques have significantly advanced simple proof-of-concept ideas of hyperpolarized MRS/MRI into clinical applications.

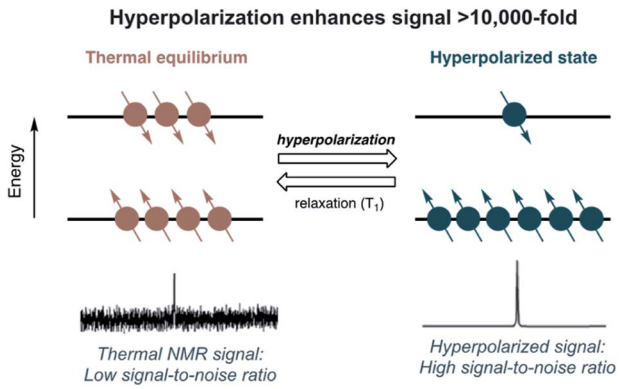


Fig. 1 Hyperpolarization of the nuclear-spin population to enhance NMR signals.

### 1.3. Development of hyperpolarized MRI/MRS agents: considering factors and current progress

Hyperpolarized imaging studies rely on molecular probes, which are isotope-enriched chemical agents used to visualize, characterize, and quantify biological processes.[18,19] These probes can be fine-tuned to characterize a specific molecular or cellular process of interest for diagnostic or therapeutic applications. Developing an effective hyperpolarized molecular imaging probe is challenging, particularly in addressing several important considerations that are specific to hyperpolarized imaging. First, the labeled nuclei should have a long longitudinal relaxation time, denoted as $T_1$. The MR signal detection window strictly depends on the $T_1$ value, which represents approximately 1/3 of polarization decay back to the thermal equilibrium of the spin population. Therefore, great efforts have been devoted to extending the polarized state in the hyperpolarization process and identifying isotope-labeled functional groups and centers with long $T_1$ lifetimes. For example, $^{13}C$ centers without directly attached protons, such as $^{13}C$ centers in carbonyl groups, benefit from the decreased dipolar relaxation and commonly have longer $T_1$ values.[20]

In addition to the dipolar contribution, the magnetic field strength also affects the $T_1$ value. The magnetic field strength, commonly measured in tesla (T), correlates with the signal-to-noise ratio – a stronger magnetic field yields stronger signals over background noise and consequently, provides a better image. Routinely used clinical MRI scanners have field strengths of 1.5 and 3.0 T, while research MRI and laboratory

NMR spectrometers commonly have field strengths of 7.0, 11.7, and 14.1 T. Generally, the $T_1$ has an inverse correlation with the magnetic field, so the higher fields result in shorter $T_1$ values.

Second, the design of HP-MR probes should consider the difference in the chemical shift between the probe and its reaction product (*i.e.*, metabolite). A larger chemical shift difference in the NMR spectra will provide more distinguishable peak identification and quantification, especially in lower magnetic fields (for example, typically 5–40 ppm for $^{13}$C).[21]

In the current field of HP imaging, $^{13}$C tracers are the most explored for studying metabolic processes, largely because carbon serves as a backbone for nearly all organic biomolecules. Several comprehensive review papers delineate hyperpolarized $^{13}$C probes exploited for preclinical and clinical research,[20–28] which is beyond the scope of this review paper. The success in hyperpolarized $^{13}$C imaging has validated the applicability of HP MRI/MRS technology in clinical settings for monitoring disease progression and therapy response. At the same time, $^{13}$C-labeled agents often manifest short polarization lifetimes, with $T_1$ values of only tens of seconds, presenting a limitation for imaging slower biological processes beyond rapid metabolic systems.

Compared to $^{13}$C-based probes, hyperpolarized $^{15}$N agents have proved to offer much longer $T_1$ lifetimes and are well suited for sensor designs.[29] This review will present current accounts of hyperpolarized $^{15}$N-labeled biomolecular probes studied in the literature, the advantages and challenges associated with $^{15}$N-probes, and how $^{15}$N-agents can provide unique directions in the field of hyperpolarized imaging.

# 2. Hyperpolarized $^{15}$N probes

## 2.1. Introduction on $^{15}$N-labeled probes: unique properties and potential in molecular imaging

Nitrogen atoms are present ubiquitously in bioorganic molecules, and in principle, any nitrogen center can be isotope-enriched with $^{15}$N nuclei.[30] As $^{15}$N has a gyromagnetic ratio lower than those of $^{1}$H and $^{13}$C, the $^{15}$N-NMR signal suffers from poorer sensitivity. However, the reduced interaction of $^{15}$N with an external magnetic field allows longer polarization lifetimes of $^{15}$N centers in the order of several minutes. Such long polarization lifetimes expand the imaging window of the hyperpolarized species and dramatically broaden the potential applications in biomedical imaging beyond rapid metabolism tracing restricted by the shorter $T_1$ lifetime of $^{13}$C metabolites.

Besides potentially long hyperpolarized lifetimes of the $^{15}$N nucleus, $^{15}$N-NMR has a wider range of chemical shifts. This warrants a greater sensitivity of $^{15}$N chemical shift to its environment. The development of non-$^{1}$H-based MRI and MRS agents has been partially motivated by the difficulty in deconvoluting many metabolite resonances in the narrow chemical shift range of ~10 ppm of the $^{1}$H spectrum. In comparison, peaks corresponding to $^{13}$C metabolites of interest occur over a much wider range of approximately 200 ppm. A wider range of chemical shifts provides hyperpolarized $^{13}$C-based probes with greater qualitative analysis capability to trace complex biochemical processes. In this respect, the $^{15}$N spectrum provides an even more comprehensive range up to 900 ppm,[29] thus providing hyperpolarized $^{15}$N probes with an even higher detection accuracy and an extended scope of chemical complexity. These favorable features of hyperpolarized $^{15}$N-probes offer promising biomedical and clinical imaging applications.

This review presents the up-to-date progress in the development of various $^{15}$N agents for hyperpolarized bioimaging. The HP $^{15}$N agents reported so far are classified into three main categories in this review: (1) $^{15}$N-enriched endogenous molecules and drugs, (2) $^{15}$N sensors designed for specific physiological parameters, and (3) biomolecules labeled with $^{15}$N molecular tags. The discussion on these probes generally covers the design principles, considerations, and imaging performances in each molecular probe category.

## 2.2. $^{15}$N-Enriched endogenous molecules and drugs

Isotope enrichment is the most straightforward approach in designing HP agents, including $^{15}$N-labeled endogenous metabolites and drug molecules. Ideally, HP agents should have low toxicity and high cellular uptake for *in vivo* imaging. Considering that the imaging agents are typically hyperpolarized *ex vivo* and injected intravenously into animals, high concentrations of HP agents (generally 10–100 mM) are often needed, taking into account the dilution in the blood, to produce sufficiently detectable NMR signals *in vivo*. The cytotoxicity profiles of endogenous metabolites and drug molecules are readily available, which expedited the *in vivo* applications of $^{15}$N-enriched hyperpolarized probes. So far, several successful probes in this regard have been reported, including $^{15}$N-choline, $^{15}$N-permethylated amino acids, $^{15}$N-carnitine, $^{15}$N-azidothymidine (AZT), and $^{15}$N-heterocycle-based drugs.

**2.2.1. $^{15}$N-Choline.** Choline (Cho) is an endogenous molecule involved in phospholipid metabolism. Elevated metabolism of choline to phosphocholine (PCho) catalyzed by choline kinases is a known characteristic of cancer, making choline an ideal biomarker for tumor imaging.[31,32] None of the carbon centers in the natural choline molecule $(CH_3)_3N^+CH_2CH_2OH$ would retain a long $T_1$ lifetime if $^{13}$C-enriched. However, the quaternary amine is suitable for $^{15}$N-enrichment to achieve long-lasting polarization, benefiting from the absence of proton-based dipole relaxation.

$^{15}$N-Enriched choline has been hyperpolarized and studied to monitor *in vitro* choline metabolism to $^{15}$N-PCho for the first time by Gabellieri *et al.* (Fig. 2A).[33] The non-basic and symmetrical environment of the quaternary $^{15}$N center in choline led to exceptionally long $T_1$ values of 285 ± 12 s in water and 120 ± 10 s in blood at 37 °C in a magnetic field of 11.7 T. A reduction of $T_1$ in the blood is a documented phenomenon and can result from the increased relaxation caused by the viscosity of blood, presence of red blood cells, and hydrogen-bonding with biomolecules. This study monitored the *in vitro* enzymatic conversion of hyperpolarized $^{15}$N-Cho to $^{15}$N-PCho, with a maximum buildup of $^{15}$N-PCho observed at 114 s. The initial rate of $^{15}$N-PCho buildup was estimated to be 1.45 mM min$^{-1}$ using choline kinase (2 μM). Such kinetics information

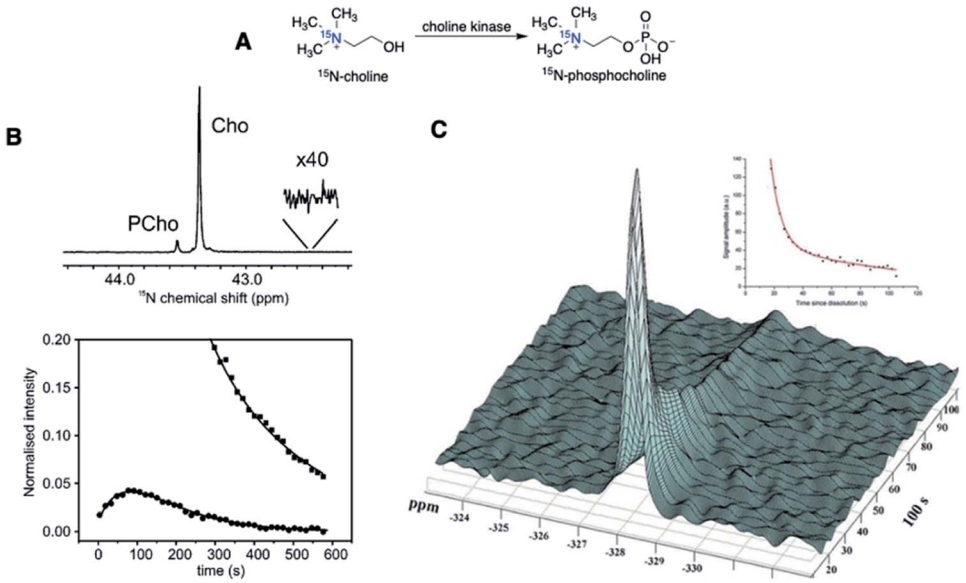


Fig. 2 First hyperpolarization experiments of $^{15}$N-choline. (A) Schematic conversion of $^{15}$N-choline to $^{15}$N-phosphocholine. (B) (Top): Enzymatic conversion of hyperpolarized $^{15}$N-Cho to $^{15}$N-PCho, scanned at the maximum buildup PCho ($t$ = 114 s, $\Delta^{15}$N = ~0.2 ppm), and (bottom): peak integral plotted against imaging time in seconds, with squares = $^{15}$N-Cho and circles = $^{15}$N-PCho. (C) First *in vivo* polarization decay graph of $^{15}$N-Cho spectra, with the $^{15}$N peak referenced to nitromethane. (B) Adapted with permission from ref. 33. Copyright 2008, American Chemical Society. (C) Adapted with permission from ref. 35. Copyright 2010, The Royal Society of Chemistry.

obtained using the plotted hyperpolarization signal over time is vital for estimating substrate buildup rates and enzyme activity. Most encouragingly, the $^{15}$N signal remained after 10 min, substantially exceeding the longevity compared to deuterated $^{13}$C-choline with a $T_1$ of ~30 s (11.8 T).[34] On the other hand, the $^{15}$N spectra of $^{15}$N-Cho and $^{15}$N-PCho showed a chemical shift difference of only ~0.2 ppm. Such a small difference presents a challenge for practical *in vivo* imaging of choline kinase activity, especially with low sensitivity of the $^{15}$N nucleus at clinically relevant MRI (3 T) (Fig. 2B).[33] Nonetheless, the exceptionally long relaxation time of $^{15}$N-choline in these earlier studies showed great promise in hyperpolarized $^{15}$N imaging and has drawn scientific attention to exploring a new range of biological applications.

In 2012, Cudalbu *et al.* performed MRS of HP $^{15}$N-Cho to monitor $^{15}$N-Cho build-up in a rat brain. This *in vivo* study has established the feasibility of detecting hyperpolarized $^{15}$N signals in the animal model for the first time.[35] Injection of $^{15}$N-choline infusate at ~90 mM was tolerated without severe toxicity, although previous work has reported that MRI of choline was problematic due to its toxicity at high doses.[36] As shown in Fig. 2C, hyperpolarized $^{15}$N-Cho provided a $T_1$ of 126 ± 15 s *in vivo* (9.4 T) and the $^{15}$N-Cho signals were detectable well over 100 s, possibly over 300 s based on the $T_1$ value. However, the choline kinase activity was not observed in the animal model, possibly owing to the decreased sensitivity of the $^{15}$N signal *in vivo* and slow Cho uptake.

Promising potential of hyperpolarized choline in diverse applications has also attracted efforts to improve hyperpolarization efficiency and lifetimes of $^{15}$N-Cho, for example, by a deuteration strategy (Fig. 3). A study by Sarkar *et al.* showed that naturally abundant choline-$d_9$ with deuterated methyl groups showed a $T_1$($^{15}$N) of 390 ± 110 s, and $^{15}$N-Cho showed a $T_1$ of 189 ± 2 s (both in $D_2O$ at 7 T).[37] Note that compared to 285 ± 12 s (11.7 T) in Gabellieri *et al.*,[33] the shorter relaxation of $^{15}$N-Cho shown in Sarkar's study was due to the addition of free radicals used for d-DNP hyperpolarization. In another study by Kumagai *et al.*, the fully deuterated $^{15}$N-choline-$d_{13}$ showed a $T_1$ of 580 ± 10 s (9.4 T).[38]

Similarly, a $^{15}$N-choline analog has been hyperpolarized using PHIP in aqueous media, achieving a $T_1$ of 348 ± 10 s and 494 ± 13 s for protonated and deuterated substrates, respectively (9.4 T).[39] Longer relaxation times of hyperpolarized $^{15}$N signals in these deuterated choline analogs were rationalized by the reduced dipolar relaxation pathway with every neighboring proton (spin = $\frac{1}{2}$) replaced with deuterium (spin = 1). These studies also demonstrate that the deuteration of nearby protons can increase the polarization lifetime of $^{15}$N ammonium centers up to 3-fold.

**2.2.2. Permethylated, perdeuterated $^{15}$N-amino acids.** $^{15}$N-Enriched derivatives of amino acids, another type of endogenous molecules, have been studied extensively for long-lasting hyperpolarized perfusion imaging. Specifically, the $^{15}$N-


Fig. 3 Structures of $^{15}$N-cholines with various degrees of deuteration, showing deuteration of the methyl and methylene groups of choline elongates the $T_1$ lifetime.

enriched amino acids can perform as tracers to study renal functions, such as filtration rates and tubular properties that are vital for diagnosing metabolic disorders.

Chiavazza *et al.* have first prepared permethylated, perdeuterated derivatives of glutamine, glutamate, and lysine.[40] The design of perdeuterated glutamine compounds was based on the long relaxation time previously observed for deuterated ammonium centers that benefit from the reduced dipolar interaction with neighboring protons. The α-glutamine-$^{15}$N, prepared by $^{15}$N-enrichment of α-amine ($^{15}NH_2$) in naturally occurring amino acids, had a $T_1$ value of merely 8 s (14.1 T). In comparison, perdeuteromethylation of α-$^{15}$N-amine in amino acids as a strategic approach dramatically increased the $T_1$ values up to 220–250 s (Fig. 4A).

Durst *et al.* applied the amino acid derivative $(CD_3)_3{}^{15}N^+$Gln to compare the hyperpolarized imaging performances of $^{15}$N-probes and $^{13}$C-urea in HP-MRI perfusion studies (Fig. 4B and C).[41] The signal from the $^{15}$N-glutamine analog was localized to the kidney area and detectable for more than 5 minutes. In contrast, the $^{13}$C signal from [$^{13}$C, $^{15}N_2$]urea was delocalized around the tissue and disappeared within 90 s (Fig. 4B). In practice, the hyperpolarized signal of $^{15}$N had a lower SNR than that of $^{13}$C, as the SNR correlates with the gyromagnetic ratio (Fig. 4C). However, this was offset by the slow signal decay of the $^{15}$N-glutamine analog in the order of several minutes.

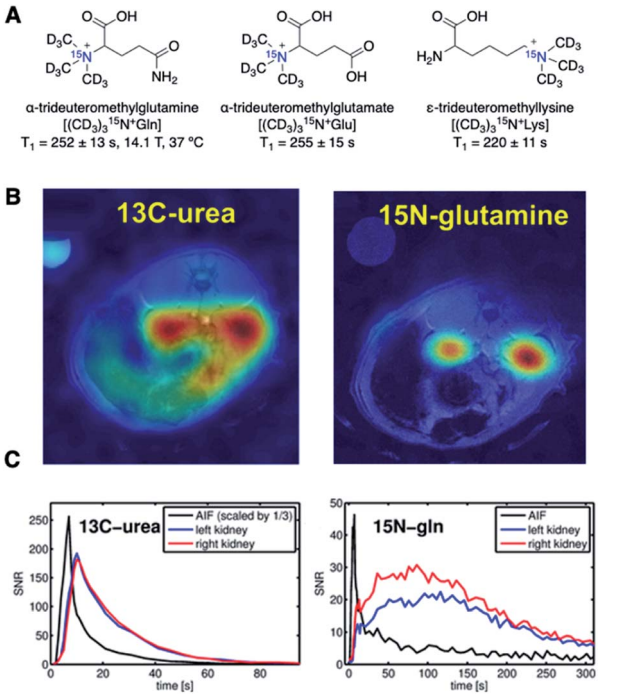


Fig. 4 (A) Structures of perdeuteromethylated $^{15}$N glutamine, glutamate, and lysine analogs. $T_1$ values of all three analogs were measured at 14.1 T and 37 °C. (B) HP-MRI of [$^{13}$C, $^{15}N_2$] urea (left) and $(CD_3)_3{}^{15}N^+$Gln (right) at the peak of signal accumulation. Image laid over $^1$H MRI, demonstrating the localized $^{15}$N-glutamine signal in the kidneys. (C) Plot of the signal-to-noise ratio (SNR) of $^{13}$C-urea and $^{15}$N-glutamine signals over a time course from kidney and blood vessel regions. (B and C) Adapted with permission from ref. 41. Copyright 2016, John Wiley and Sons.

These permethylated, perdeuterated amino acid analogs had long signal retention and showed minimal toxicity in an animal model, meeting the requirements for *in vivo* imaging applications of hyperpolarized probes. The high $T_1$ values and strong localization properties make perdeuteromethylated $^{15}$N probes promising candidates for perfusion imaging. These examples also reinforce design principles to increase $T_1$($^{15}$N) by reducing the dipolar interaction with neighboring protons and installing a symmetrical environment of the $^{15}$N nucleus.

**2.2.3. $^{15}$N-Carnitine.** The ideal HP properties of quaternary $^{15}$N centers are further illustrated by $^{15}$N-labeled L-carnitine,[42] an endogenous metabolite involved in acetyl-coenzyme A and fatty acid metabolism (Fig. 5A). The $T_1$ times of L-$^{15}$N-carnitine-$d_9$ were determined to be 210 s in water and 160 s *in vivo* (4.7 T) (Fig. 5B). Furthermore, the MR spectroscopic imaging of HP $^{15}$N-carnitine in the rat abdomen three minutes after injection showed $^{15}$N signals localized in the liver and kidney area, proving the feasibility of imaging the biodistribution of an $^{15}$N-agent for an extended period (Fig. 5C–E). However, no downstream $^{15}$N-acetyl-carnitine metabolites were detected in this study due to magnetic isolation of the $^{15}$N-quaternary atom.

The $^{15}$N-labeled choline, amino acids, and carnitine studies show several benefits of simple isotope-enrichment of endogenous molecules, such as ease of synthesis, high aqueous solubility, and low cytotoxicity. Nonetheless, $^{15}$N-labeled endogenous molecules do not present detectable chemical reactions and thus cannot capture real-time physicochemical activities. Discovery of imaging agents that undergo an enzymatic or chemical reaction with significant $^{15}$N chemical shift differences will provide even greater analytical appeal in terms of structure determination and quantification.

**2.2.4. $^{15}$N-Azidothymidine (AZT).** $^{15}$N-Enrichment of nitrogen-containing drug molecules may offer the capability of monitoring the drug's location and metabolism by HP imaging. A good example of this category is azidothymidine (AZT), an azide-containing antiviral drug that prevents reverse transcriptase from forming viral DNA.[43] Shchepin *et al.* have reported the synthesis of AZT using sodium-$^{15}N^{14}N_2$ azide to yield singly labeled $^{15}N^{14}N_2$-AZT as a mixture of 1-$^{15}$N and 3-$^{15}$N isotopomers. This mixture of 1-$^{15}$N and 3-$^{15}$N labeled AZT provided two distinct hyperpolarized $^{15}$N NMR peaks.[44] SABRE hyperpolarization provided $T_1$ values of 1-$^{15}$N and 3-$^{15}$N azides as 45 ± 1 and 37 ± 2 s, respectively (9.4 T) (Fig. 6A). In another study by Bae *et al.*, triply labeled $^{15}N_3$-AZT and singly labeled $^{15}N^{14}N_2$-AZT hyperpolarized by d-DNP showed $T_1$ values of 2.5–5.3 min (1 T).[45] In this study, the singly labeled 1-$^{15}$N center was affected by the scalar relaxation with neighboring $^{14}$N ($I = 1$), leading to unmeasurable $T_1$ at 1 T. These studies exemplify the synthesis of $^{15}$N-labeled drug molecules with the potential to monitor drug activities.

**2.2.5. $^{15}$N-Nicotinamide and $^{15}$N-dalfampridine.** Hyperpolarized $^{15}$N-heterocycles have been explored as potential drug contrast agents. Nicotinamide, also known as vitamin B3 amide, is a drug that is used for the treatment of *M. tuberculosis*, HIV and cancer.[46,47] Shchepin *et al.* have demonstrated an efficient synthesis of $^{15}$N-enriched nicotinamide with high isotopic purity.[48] SABRE-SHEATH (SHield Enables Alignment Transfer to

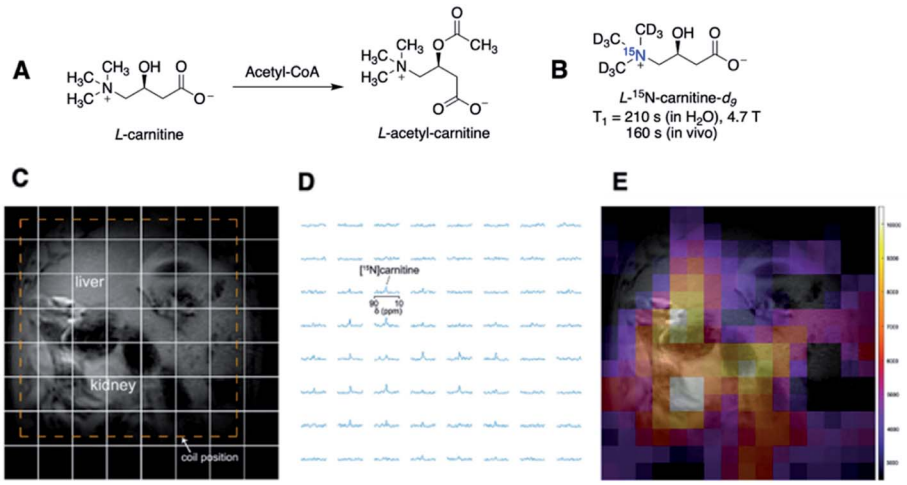


Fig. 5 (A) Structures of endogenous L-carnitine and its acetylated product. (B) $T_1$ lifetimes of L-$^{15}$N-carnitine-$d_9$ in water and *in vivo*. (C) Spectral grid used for MR imaging overlaid on the $^1$H anatomic image. (D) $^{15}$N spectra of each spectral grid (E) hyperpolarized $^{15}$N-carnitine signals in color overlaid on the anatomic image, illustrating the biodistribution of $^{15}$N-carnitine in the liver and kidney. (C–E) Adapted with permission from ref. 42. Copyright 2020, John Wiley and Sons.

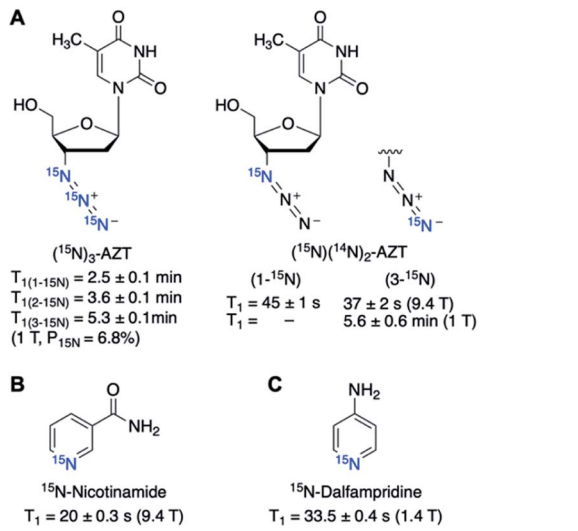


Fig. 6 Structures and hyperpolarized lifetimes of (A) singly and triply labeled $^{15}$N-AZT, (B) $^{15}$N-nicotinamide, and (C) $^{15}$N-dalfampridine.

Heteronuclei) hyperpolarization of $^{15}$N-nicotinamide provided a $T_1$ of 20.2 ± 0.3 s (9.4 T), presenting the possibilities of synthesized $^{15}$N-heterocycles as hyperpolarized drug contrast agents. Similarly, dalfampridine (4-aminopyridine) is another pyridine-based drug used to treat the symptoms of multiple sclerosis.[49] In a study by Chukanov *et al.*, $^{15}$N-enriched dalfampridine has been synthesized and hyperpolarized with SABRE-SHEATH to afford a $T_1$ of 33.5 ± 0.4 s (1.4 T).[50] These studies illustrate the significance of $^{15}$N-enrichment methodology development for biomedical applications.

The feasibility of hyperpolarized $^{15}$N-drug imaging is yet to be confirmed with *in vivo* studies. In addition to hyperpolarization efficiency, factors such as drug metabolism rate, cellular uptake, and cytotoxicity of the probe of interest need to be scrutinized to meet the criteria for preclinical applications.

**2.2.6. $^{15}$N-Nitrate.** Hyperpolarized $^{15}$N-nitrates ($^{15}NO_3^-$), bioactive ions that mediate physiological processes, have been explored as contrast agents for HP-MRI. D-DNP hyperpolarization of $^{15}$N-nitrate in $D_2O$, $H_2O$ and saline provided $T_1$ values of ~100 s for each solvent at a temperature range of 34–44 °C, which was reduced to a $T_1$ of 29 ± 1 s in blood samples. The metabolic conversion from $^{15}$N-nitrate to $^{15}$N-nitrite was undetectable in blood and saliva, making this molecular probe suitable as an MR tracer for perfusion or tissue retention imaging.[51]

### 2.3. $^{15}$N-Labeled molecular sensors for detecting the biological environment

Most nitrogen centers in biomolecules are proton-bound amines or amides, in which hyperpolarized $^{15}$N signals would suffer shortened lifetimes, owing to the dipole relaxation pathway. This challenge associated with short $T_1$ has limited the range of HP $^{15}$N-labeled endogenous molecules to quaternary permethylated $^{15}$N-centers, such as the $^{15}$N-choline and amino acid derivatives. However, *de novo* $^{15}$N molecular probes not restricted to endogenous biomolecules present great promise as chemical sensors. Several examples of $^{15}$N-labeled chemical sensors have been reported so far for the detection of intracellular pH, signaling molecules, and enzymatic activity as potential disease biomarkers.

**2.3.1. $^{15}$N-Heteroatom bases as pH sensors.** Imbalanced intracellular pH is closely related to pathological processes and is a hallmark for diseases such as cancer.[52] Developing pH sensors for effective cancer diagnosis has attracted continuous interest, including isotope-labeled hyperpolarized pH sensors. Several $^{13}$C-pH sensors have been developed, such as [1-$^{13}$C]-bicarbonate[53,54] and $^{13}C_2$-zymonic acid,[8] allowing for pH detection *via* the proton exchange of $^{13}$C-carboxylic acids.

Alternatively, $^{15}$N-based pH sensors have been developed for direct $^{15}$N-protonation-based chemical shift imaging because sp$^2$-hydridized, aromatic nitrogen centers can be protonated near physiological pH and cause significant electronic changes in the $^{15}$N atom.

Jiang *et al.* first illustrated hyperpolarized $^{15}$N-pyridine and pyridine derivatives as potential pH sensors (Fig. 7A and B).[55] $^{15}$N-Pyridine demonstrated pH-sensitive chemical shift changes up to 90 ppm at a pH range of 2.1–8.5. Sharper chemical shift changes were observed in pH near a $^{15}$N-pyridine p$K_a$ of 5.17, and the pH sensitivity was further altered by adding substituents to the pyridine derivatives. Yet the $^{15}$N-pyridines suffered from a short hyperpolarization lifetime, with a $T_1$ value of 41 s for non-protonated $^{15}$N-pyridine (pH 8.4) that decreased to 11 s in plasma (9.4 T). The reduced $T_1$ is due to an added relaxation pathway from proton exchange between the $^{15}$N atom (H–$^{15}$N$^+$) and water.

A study by Shchepin *et al.* examined $^{15}N_2$-imidazole as a pH sensor by SABRE-SHEATH hyperpolarization (Fig. 7C and D).[56] $^{15}N_2$-Imidazole, with a p$K_a$ of ~7.0, showed higher sensitivity near physiological pH than that of $^{15}$N-pyridine, with a chemical shift change of ~15 ppm within the range of 6.5–7.5 (1.5 ppm/0.1 pH unit). $^{15}N_2$-Imidazole demonstrated a $T_1$ value of only 24 s in 1 : 1 MeOH : $H_2O$ (9.4 T). Although the $T_1$ measurements at the physiological pH were not disclosed, $^{15}N_2$-imidazole is expected to have faster signal decay upon protonation, based on the results from $^{15}$N-pyridine. Similarly, a simultaneous hyperpolarization of cleavable $^{15}N_2$-imidazole and $^{13}$C-acetate has been reported, exemplifying the possibility of dual $^{15}$N/$^{13}$C-labeled HP agents for metabolic and pH sensing.[57]

These studies use isotope-enriched substrates because of the low natural abundance of $^{15}$N (0.37%). Notably, high levels of $^{15}$N polarization of naturally abundant substrates (*i.e.*, pyridine, metronidazole and acetonitrile) up to $P_{15N} = 51\%$ have been achieved using SABRE hyperpolarization in the presence of amines as coligands of the SABRE catalyst. Such a study will allow simple and efficient hyperpolarization of nitrogen-containing pH sensors and relevant biomolecules for $^{15}$N-MRI.[58]

**2.3.2. $^{15}$N-TMPA for detection of ROS and enzyme activity.** Unlike the above-mentioned $^{15}$N-based pH sensors designed with an all-in-one $^{15}$N-sensing and signaling unit, the probes can be designed with a separate sensing unit and a signal unit. In this alternative design, the sensing unit surveys a biological system of interest while a remote $^{15}$N signaling unit provides chemical shift changes as a readout.

Nonaka *et al.* exemplified this design strategy in [$^{15}$N]trimethylphenylammonium ($^{15}$N-TMPA) as a versatile platform for developing $^{15}$N-based sensors that can potentially adapt any sensing of interest.[59] At the same time, $^{15}$N-TMPA can provide a long polarization lifetime of the quaternary permethylated $^{15}$N center, with minimal influence on $T_1$ from the environment. In this study, the $^{15}$N-TMPA imaging platform was examined for a reaction-based detection of $H_2O_2$ and carboxyl esterase, the representative reactive oxygen species and enzyme commonly elevated in diseases (Fig. 8A and C). Both probes showed $H_2O_2$ concentration or enzyme-activity-dependent $^{15}$N-chemical shift changes. Deuterated [$^{15}$N, $d_9$]-TMPA offered a $T_1$ of over ~7 min (9.4 T). Such a long polarization lifetime allowed for an extended $^{15}$N signal detection of up to 40 min, considering that the $T_1$ value is approximately 37% of the total hyperpolarization decay. However, both $H_2O_2$ oxidation or carboxyl esterase

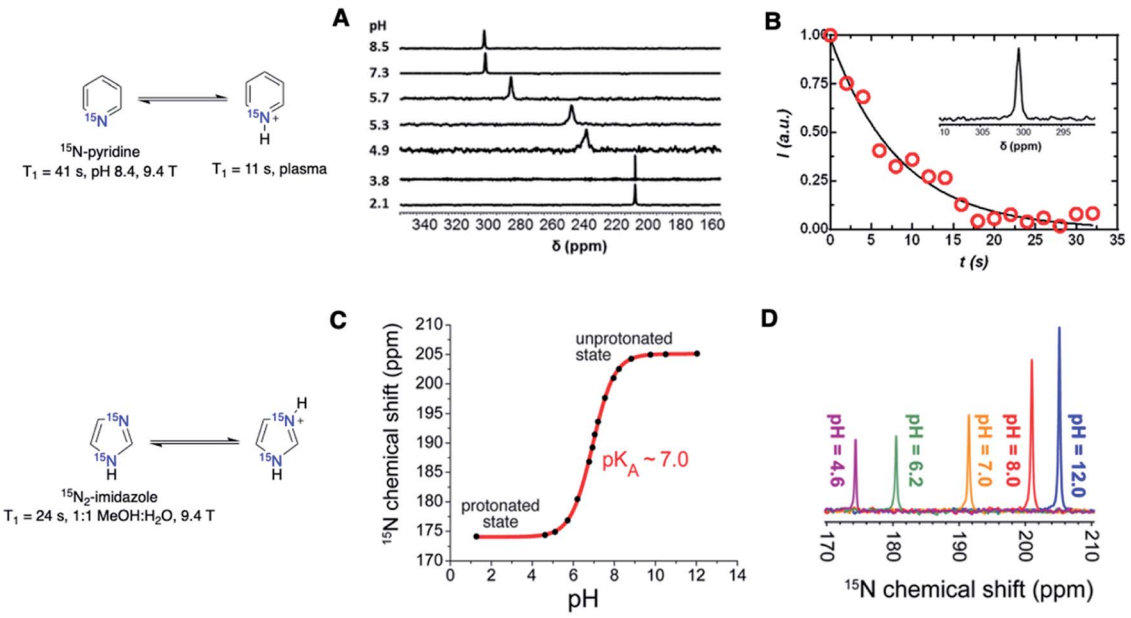


Fig. 7 (A) pH-dependent $^{15}$N chemical shifts of free-base and protonated $^{15}$N-pyridine. (B) Hyperpolarization signal decay of $^{15}$N-pyridine in rat plasma with a $T_1$ value of ~11 s. (C) Determination of $^{15}N_2$-imidazole p$K_a$ using $^{15}$N chemical shifts. (D) Chemical shifts of thermally polarized $^{15}N_2$-imidazole in water at various pH values. (A and B) Adapted with permission from ref. 55. Copyright 2015, Springer Nature. (C and D) Adapted with permission from ref. 56.

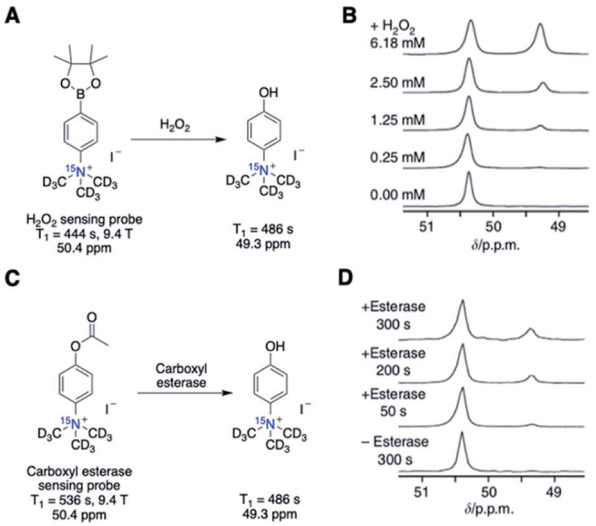


Fig. 8 (A) Scheme of $H_2O_2$ detection probe reaction. (B) Scans of the hyperpolarized $H_2O_2$ detection probe in the presence of various concentrations of $H_2O_2$ (in PBS, 50 s after mixing). (C) Scheme of carboxyl esterase detection probe reaction. (D) Scans of the hyperpolarized carboxyl esterase detection probe in the presence of esterase (125 units $mL^{-1}$ in PBS). (B and D) Adapted with permission from ref. 59. Copyright 2013, Springer Nature.

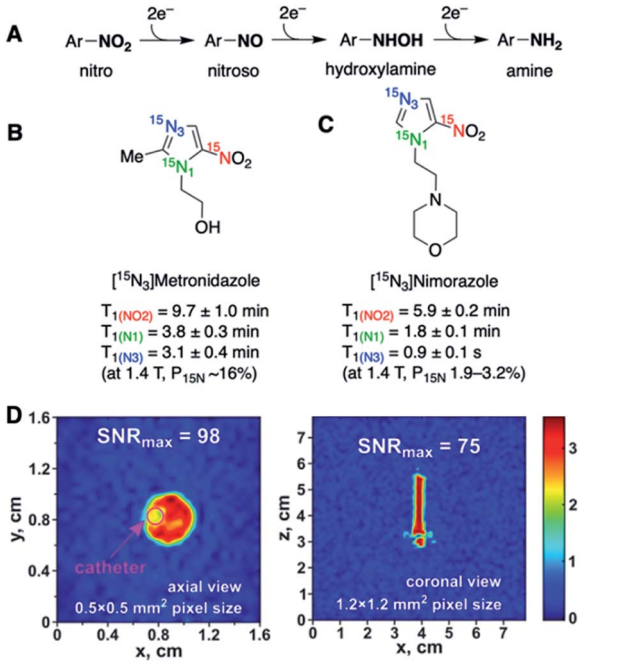


Fig. 9 (A) Schematic illustration of sequential nitro reduction under hypoxic conditions. (B) $T_1$ lifetimes of the three $^{15}N$ centers in $^{15}N$-labeled metronidazole. (C) $^{15}N$-Labeled nimorazole as a hyperpolarized imaging agent of hypoxia. (D) 2D sub-second $^{15}N$ MRI visualization of HP [$^{15}N_3$]nimorazole in a 5 mm NMR tube (9.4 T). Axial (left) and coronal (right) projections of the first scan of $^{15}N$ MRI. (D) Adapted with permission from ref. 63. Copyright 2020, John Wiley and Sons.

reaction of [$^{15}N$, $d_9$]-TMPA resulted in a $^{15}N$ shift difference of merely ~1.5 ppm (Fig. 8B and D). Such a small chemical shift difference corresponds to a $^{15}N$ frequency of only 60 Hz at 9.4 T and even smaller at clinically relevant magnetic fields, with 19 Hz at 3 T and 9.7 Hz at 1.5 T, which would be insufficient for signal distinction. These results suggest that a $^{15}N$ chemical shift change of larger than 1.5 ppm is needed to distinguish the peaks for accurate analysis of the signals.

The excitingly long $T_1$ values in these $^{15}N$-based probes significantly broaden the HP imaging possibilities for *in vivo* characterization of slower biochemical reactions, such as enzymatic reactions, redox activities, and cellular signaling pathways, which would be otherwise challenging with a short signal lifetime of HP $^{13}C$-probes.

**2.3.3. $^{15}N$-Metronidazole and $^{15}N$-nimorazole as hypoxia sensors.** $^{15}N$-Labeled probes for hypoxia sensing have been developed as an imaging model of the tumor microenvironment. Hypoxia, a condition with inadequate oxygen supply in tissues, is a common feature in solid tumors and a diagnostic marker for therapy-resistant tumors.[60] Thus, non-invasive and reliable hyperpolarized hypoxia sensors offer valuable tools for cancer diagnosis and predicting therapy efficacy.

Nitroimidazoles have been widely used as hypoxia markers through immunohistochemistry and PET imaging. Under hypoxic conditions, the nitro group of these nitroimidazole compounds is expected to undergo sequential bioreduction to form nitroso, hydroxylamine, and amine derivatives (Fig. 9A). These hypoxia-based reactions can potentially provide significant $^{15}N$ chemical shift changes and make $^{15}N$-nitroimidazoles suitable candidates for MRS/MRI probes. So far, two types of $^{15}N$-labeled nitroimidazoles have been investigated as hypoxia sensors.

Metronidazole is an FDA-approved nitroimidazole-type antibiotic drug. It can be administered safely at high doses, which well suits the use of hyperpolarized solution at high concentrations for HP-MR studies. Efficient hyperpolarization of naturally abundant metronidazole[61] as well as $^{15}N$-enriched [$^{15}N_3$]-metronidazole[62] has been demonstrated using SABRE--SHEATH. In the work by Shchepin *et al.*, all three $^{15}N$ sites had high polarizations of ~16% and long polarization lifetimes (Fig. 9B).[62] Among the three $^{15}N$ centers, $^{15}NO_2$ had an extraordinarily long $T_1$ value of 9.7 min (1.4 T), and the two aromatic $^{15}N$-1 and $^{15}N$-3 centers in the imidazole ring had $T_1$ values of 3.1 and 3.8 min, respectively. Nimorazole is another imidazole-based radiosensitizer drug for head and neck cancer. [$^{15}N_3$]-Nimorazole has also been studied as a potential HP sensor for tumor hypoxia. Salnikov *et al.* reported hyperpolarized [$^{15}N_3$]-nimorazole as a potential theranostic agent for dual therapy and imaging of tumor hypoxia (Fig. 9C).[63] Hyperpolarization of [$^{15}N_3$]-nimorazole using SABRE-SHEATH provided long $T_1$ lifetimes, especially for $^{15}NO_2$ (5.9 min, 1.4 T). Such remarkably long-lasting polarizations open opportunities for hyperpolarized hypoxia MR imaging for over tens of minutes.

Although neither of these two studies have reported metabolic imaging of $^{15}N$-nitroimidazoles, the *ab initio* calculations

revealed that the sequential hypoxic reduction processes shown in Fig. 9A were expected to provide significant $^{15}$N chemical shift differences, with nearly 800 ppm difference for the $^{15}$N-nitro center.[63] Such a dynamic chemical shift range of the $^{15}$N-sites bodes well for future *in vivo* imaging of nitroimidazole metabolism. One challenge is that the $^{15}NH_2$ metabolite from hypoxic reduction would deliver a short $T_1$ because of the proton-coupled relaxation pathway. A possible alternative readout to monitor hypoxia is the other two sp$^2$-$^{15}$N atoms that may also lead to chemical shift changes upon $^{15}NO_2$ reduction.

While *in vivo* imaging has not been demonstrated in these studies, the 2D $^{15}$N MRI visualization of [$^{15}N_3$]-metronidazole[64] and [$^{15}N_3$]-nimorazole[63] displayed high spatial and temporal resolution (Fig. 9D), highlighting the prospects of high-resolution $^{15}$N-imaging.

**2.3.4. Coordination-based detection of $Ca^{2+}$ and $Zn^{2+}$ metal ions.** MR probes have also been designed for sensing biologically important metal ions. Free metal ions, such as calcium and zinc, participate in essential cellular ionic signaling cascades and oxidative balance. The importance of metal ion homeostasis suggests the promise of *in vivo* metal ion concentrations as diagnostic markers for analyzing diseases associated with metal ion imbalance. So far, hyperpolarized sensors for metal ions have been developed by designing chelators that can coordinate to metal ions to induce electron localization and chemical shift changes.

[$^{15}$N, d$_9$]-TMPA has been studied as a potential sensor for calcium ions ($Ca^{2+}$). Calcium ions are ubiquitous signaling molecules that control various cellular functions, and abnormal $Ca^{2+}$ concentrations are responsible for several pathological processes.[65] The design of [$^{15}$N, d$_9$]-TMPA used $(CD_3)_3{}^{15}N^+$ as the signaling unit and triacetic acid branches as the $Ca^{2+}$ chelator. Unfortunately, small $^{15}$N chemical shift changes up to 1.5 ppm were inadequate for unambiguous $Ca^{2+}$ detection (Fig. 10A).[59] To address this limitation, another $Ca^{2+}$ sensor $^{15}$N-*o*-aminophenol-*N*,*N*,*O*-triacetic acid ($^{15}$N-APTRA) was designed with the $^{15}$N center positioned close to the $Ca^{2+}$ coordination site.[66] Encouragingly, $^{15}$N-APTRA provided chemical shift changes up to 5.2 ppm with the addition of 2 equivalence of $Ca^{2+}$. On the downside, $^{15}$N-APTRA showed a $T_1$ of only 37 s (pH 7.4, 9.4 T), a 3.5-fold decrease from $T_1$ = 130 s of [$^{15}$N, d$_9$]-TMPA, presumably from protonation of $^{15}$N-aniline (Fig. 10B).

$^{15}$N-Labeled sensors for $Zn^{2+}$ metals have also been reported. Elevated cellular $Zn^{2+}$ levels are highly toxic and linked to cancer and neurodegenerative disorders. Imaging labile zinc ions as biomarkers presents a promising approach for diagnosing these diseases.[67,68] $^{15}$N-labeled tris(2-pyridylmethyl)amine (TPA) was developed by Suh *et al.* using chemical shift changes resulting from pyridine–$Zn^{2+}$ coordination for the detection and quantification of free $Zn^{2+}$ metal (Fig. 10C).[69] $^{15}$N-TPA showed several promising spectral features, including a favorable $^{15}$N signal linewidth, a large chemical shift of 20 ppm, and a linear relationship of peak area to zinc concentration. $T_1$ values for [$^{15}$N]TPA-d$_6$ and $Zn^{2+}$-[$^{15}$N]TPA-d$_6$ were 71 s and 57 s, respectively (9.4 T). Excitingly, the hyperpolarized [$^{15}$N]TPA-d$_6$ probe was able to measure physiological levels of $Zn^{2+}$ (0–200 μM) in human prostate tissue homogenate and intact human prostate epithelial cells (Fig. 10D).

These studies show versatile $^{15}$N design principles through metal–ligand coordination-based chemical shift changes for

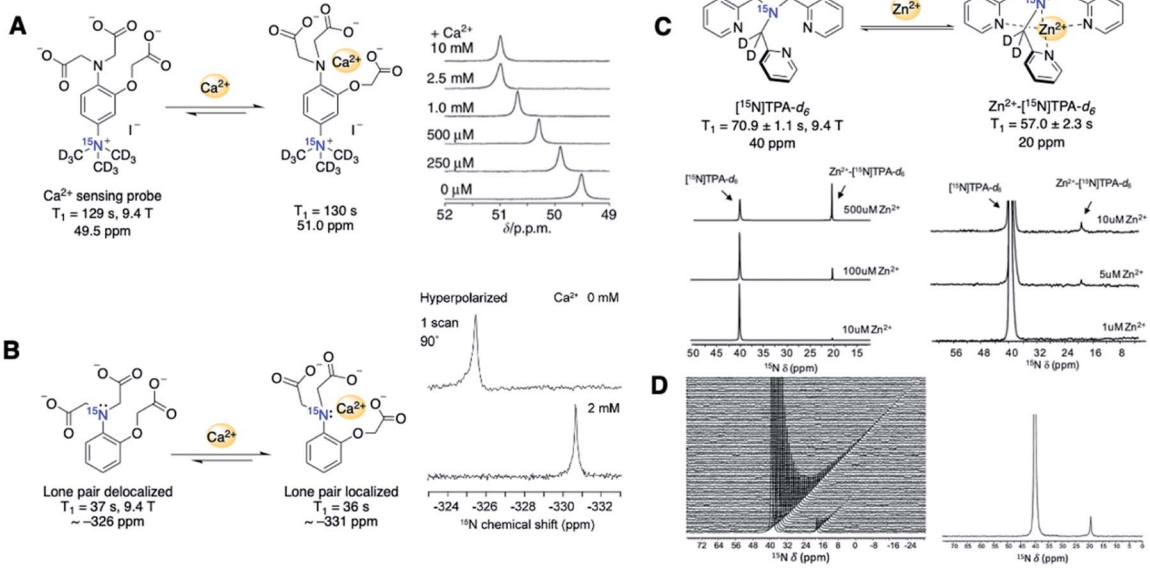


Fig. 10 (A) $^{15}$N-TMPA based $Ca^{2+}$ detection probe and $Ca^{2+}$ level-dependent $^{15}$N chemical shifts (measured in HEPES buffer, 40 s after mixing). (B) $^{15}$N-APTRA based $Ca^{2+}$ detection probe and $^{15}$N NMR spectra with and without $Ca^{2+}$. (C) [$^{15}$N]TPA-d$_6$ based $Zn^{2+}$ detection probe and $^{15}$N NMR spectra of hyperpolarized [$^{15}$N]TPA-d$_6$ (1.2 mM) with various concentrations of $Zn^{2+}$ (1–500 μM). (D) Time-dependent $^{15}$N spectra collected using intact PNT1A cells after addition of 2.8 mM of HP-[$^{15}$N]TPA-d$_6$ (left) and its first $^{15}$N spectrum showing the detection of *in vitro* $Zn^{2+}$ (right) (pH 7.4, 9.4 T). (A) Adapted with permission from ref. 59. Copyright 2013, Springer Nature. (B) Adapted with permission from ref. 66. Copyright 2015, The Royal Society of Chemistry. (C–E) Adapted with permission from ref. 69. Copyright 2020, Springer Nature.

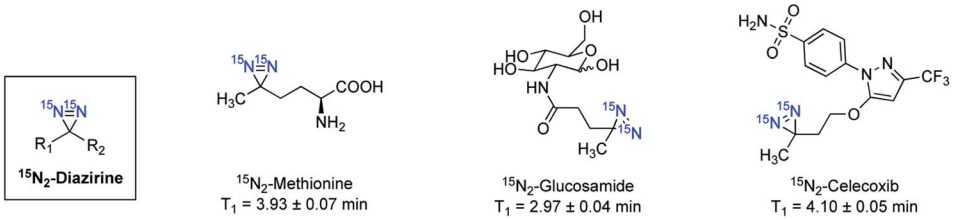


Fig. 11 Selected examples of $^{15}N_2$-diazirine-tagged endogenous and drug molecules. Hyperpolarized with d-DNP and all $T_1$ lifetimes were measured at 1 T.

hyperpolarized imaging of labile metal ions. Although a limited number of $^{15}N$ probes have been developed so far, these studies of exogenous $^{15}N$ sensors provide valuable lessons, including the effects of $^{15}N$ center placement on chemical shifts and $T_1$ values. These principles will expedite the design of more effective $^{15}N$-molecular imaging probes in future studies.

### 2.4. $^{15}N$-Molecular tags and biomolecules

An alternative to isotope enrichment, an attractive new strategy in designing HP $^{15}N$-labeled agents, is to install biocompatible and long-lasting polarized $^{15}N$-molecular tags onto biologically relevant molecules. Such a molecular tagging strategy can potentially introduce a $^{15}N$-signaling moiety into any target of interest. In the probes mentioned above, long-lived $^{15}N$ signals rely on permethylated $^{15}N$-ammonium or $^{15}N$-heterocycles as the common $^{15}N$-centers. In comparison, the $^{15}N$-molecular tags can constitute various nitrogen-containing functional groups that are non-proton bound and symmetrical, selected for optimal polarization efficiency and long-lived polarization states.

**2.4.1. $^{15}N_2$-Diazirine tags.** $^{15}N_2$-Diazirines are one of the first $^{15}N$-based molecular tags explored for HP MRS/MRI.[70] Structurally, $^{15}N_2$-diazirines are three-membered rings containing a nitrogen–nitrogen double bond (Fig. 11). Diazirines have desirable physicochemical properties for a molecular tag, including small size, biocompatibility and stability under physiological conditions, and minimal effects on the physicochemical properties of biomolecules.[71,72] Particularly attractive for HP-MR detection, $^{15}N_2$-diazirines have a unique symmetrical molecular structure that stores polarization for an extended period through a singlet state. The singlet state ($T_s$) has a zero magnetic moment, so the symmetry has to be broken to be NMR-detectable. This also means that the singlet spin order is immune to many relaxation mechanisms and polarization is long-lived. In particular, SABRE-SHEATH hyperpolarization of $^{15}N_2$-diazirine-labeled compounds had a long singlet relaxation of $T_s$ = 23 min.[70] Furthermore, several $^{15}N_2$-diazirine-labeled biomolecules have been hyperpolarized by SABRE-SHEATH[73] and d-DNP[74] methods. Examples include the $^{15}N_2$-diazirine tagged analogs of amino acids, glucose, and drug molecules. Hyperpolarization by d-DNP showed that all provided $T_1$ values in the 3–4 min range (1 T) (Fig. 11). The study showed the considerable influence of the solubility of the $^{15}N$-tagged molecules on their hyperpolarization efficiencies. High solubility of the hyperpolarized probes in the aqueous glassing solvent (at least 100 mM) is crucial for effective hyperpolarization of non-polar endogenous or drug molecules for practical applications.

**2.4.2. $^{15}N_3$-Azide tags.** Azides, unique linear species containing three nitrogen atoms, have been known as bioorthogonal reactive partners and possess desired features for a molecular tag.[75,76] $^{15}N$-Azides have been demonstrated as another class of $^{15}N$-molecular tags for hyperpolarized imaging by Bae *et al.*[45] Triply labeled $^{15}N_3$-azides have been incorporated into choline, glucose, and tyrosine analogs for investigation. Hyperpolarization of all these $^{15}N_3$-tagged molecules by d-DNP demonstrated long lifetimes up to 9.8 min (1 T) (Fig. 12). The terminal nitrogen, $^{15}N\gamma$, retained the longest HP signal, followed by $^{15}N\beta$ and $^{15}N\alpha$, in which the long $T_1$ corresponds to increased distance from the nearest protons. The $^{15}N_3$-azide tag is especially interesting as three distinct $^{15}N$ signals can be monitored simultaneously. Additionally, the extended imaging time window opens possibilities for $^{15}N_3$-azide bioconjugation reaction *in vivo* (*i.e.*, azide–alkyne cycloaddition) for hyperpolarized secondary labelling.

The $^{15}N$-tagging strategy demonstrated in $^{15}N$-azide and $^{15}N$-diazirine compounds will broaden the application of HP $^{15}N$

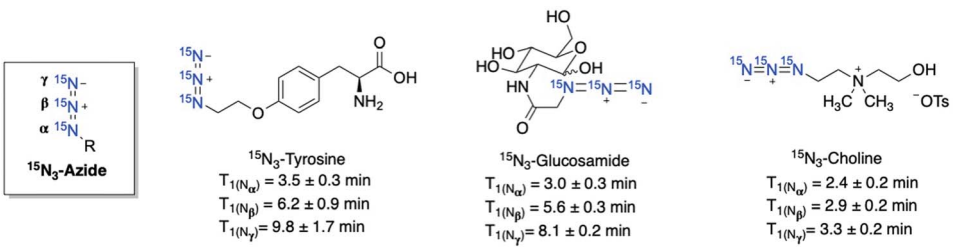


Fig. 12 Selected examples of $^{15}N_3$-azide-tagged endogenous and drug molecules. Hyperpolarized with d-DNP and all $T_1$ lifetimes were measured at 1 T.

imaging beyond nitrogen centers in heteroarenes and permethylated amines. Moreover, these $^{15}$N-tag motifs can be readily introduced into a broad range of biomolecules, allowing for preparing a variety of hyperpolarized imaging probes with a long polarization lifetime. Of note, in some examples where the $^{15}$N-tags are generally installed several bonds away from the metabolic sites, significant $^{15}$N chemical shift changes may not be observed upon metabolism. Nevertheless, the $^{15}$N-azide and $^{15}$N-diazirine-tagged molecules are of great interest for future studies on their applications in monitoring cellular uptake and accumulation.

## 3. Summary and outlook

This review provides the current state of development of HP $^{15}$N-probes, including their hyperpolarization performances in relation to design principles. As an emerging molecular imaging technique, hyperpolarized $^{15}$N MRS/MRI shows promising potential for biomedical applications. Several $^{15}$N-labeled endogenous and *de novo* molecular probes delivered long hyperpolarization lifetimes in the order of several minutes. Such substantial hyperpolarization lifetimes allow an extended imaging period to capture slower biochemical reactions that are useful for disease diagnosis. At the same time, long $T_1$ lifetimes of HP $^{15}$N agents can compensate for the low sensitivity issues, as shown in the MRS/MRI scans of $^{15}$N-amino acids and $^{15}$N-carnitine acquired over several minutes.

Despite recent progress and increased interest in $^{15}$N-based imaging in the past decade, hyperpolarized $^{15}$N MR has not gained widespread use to enter the preclinical stage. As reflected in the analysis of currently studied HP $^{15}$N-probes in this review, advancing $^{15}$N MRS/MRI into a practical imaging tool requires advancements in multiple aspects such as new probe design, extensive animal imaging studies, and improved MR technology.

Fundamental considerations for the design of novel $^{15}$N-probes include the factors of $T_1$ lifetime, chemical shift differences, and toxicity. First, the discussion on the reported $^{15}$N probes in this review reveals that the $^{15}$N signal lifetime can be greatly extended by the probe design to reduce dipole-relaxation pathways (*i.e.*, deuteration of neighboring protons). Compared to commonly observed $^{13}$C carbonyl centers, the $^{15}$N centers of the HP probes in the literature have greater structural diversity, such as quaternary amine, diazirine, and azides. All these $^{15}$N centers warrant a long $T_1$ lifetime. So far, most studies have presented polarization lifetimes at high $B_0$ (7–11.7 T). Future work on demonstrating $T_1$ in clinically relevant magnetic fields (1–3 T) will be important to accurately predict the performances of HP $^{15}$N probes in *in vivo* imaging. Second, accurate measurement of chemical reactions would require significant chemical shift differences. A serviceable chemical shift difference needed for HP imaging is affected by the magnetic field, polarization levels, and spectral resolution. Finally, the probe candidates must be biocompatible and non-toxic in living systems. The cytotoxicity profiling is critical for exogenous $^{15}$N-molecular agents, especially at high concentrations (mM range). The current exogenous $^{15}$N-probes solely demonstrate spectroscopic analysis, and only endogenous compounds (*i.e.*, $^{15}$N-choline) have advanced to *in vivo* MRI studies.

Extensive characterization of $^{15}$N-labeled agents must be performed to understand the potential use of hyperpolarized $^{15}$N imaging in clinical studies. Cellular experiments of $^{15}$N-labeled HP-NMR agents can provide information on the membrane permeability of probes and cellular reaction kinetics. Additionally, *in vivo* imaging should be conducted to validate the hyperpolarization measurements and sensitivity threshold of the $^{15}$N probes. So far, most studies have demonstrated MRS experiments. The conjunction of MRS with MRI in small animal model imaging is desirable, which will provide not only pharmacokinetic data to quantify the rate of substrate buildup and metabolite conversion but also anatomical distribution of $^{15}$N signals for accurate and quantitative analysis in preclinical studies.

Developing hyperpolarized $^{15}$N imaging for preclinical studies requires addressing several technical challenges of MR scanners' technical challenges. For instance, $^{15}$N imaging requires dedicated $^{15}$N radiofrequency coils, which are not widely available in conventional MR scanners.[69] Parallel efforts in improving pulse sequences and multichannel coils may be crucial. Advances in hyperpolarization techniques can increase polarization efficiency and address the sensitivity issues associated with $^{15}$N imaging.

Overall, the insights into the chemical and physical properties of $^{15}$N-molecular probes gained through the up-to-date examples will assist in more effective designs for future hyperpolarized $^{15}$N-based probes. Along with the advancement in MRI/MRS techniques, emerging next-generation probes are expected to foster hyperpolarized $^{15}$N-sensors as widespread molecular imaging technology in the future.

## Author contributions

Both H. P. and Q. W. contribute to the writing of this manuscript.

## Conflicts of interest

There are no conflicts to declare.

## Acknowledgements

This work was supported by NIH (R21EB024824 and P30CA014236), and the Camille and Henry Dreyfus Foundation. The content is solely the responsibility of the authors and does not necessarily represent the official views of the NIH.

## Notes and references

1 B. L. Hou and J. Hu, in *Tumor Biomarker Discovery: Methods and Protocols*, ed. M. A. Tainsky, Humana Press, Totowa, NJ, 2009, pp. 297–314, DOI: DOI: **10.1007/978-1-60327-811-9_21**.

2 J. H. Hwang and C. S. Choi, Use of *in vivo* magnetic resonance spectroscopy for studying metabolic diseases, *Exp. Mol. Med.*, 2015, **47**, e139.
3 M. van der Graaf, *In vivo* magnetic resonance spectroscopy: basic methodology and clinical applications, *Eur. Biophys.*, 2010, **39**, 527–540.
4 R. K. Harris, E. D. Becker, S. M. Cabral de Menezes, R. Goodfellow and P. Granger, NMR Nomenclature: Nuclear Spin Properties and Conventions for Chemical Shifts: IUPAC Recommendations, 2001, *Solid State Nucl. Magn. Reson.*, 2002, **22**, 458–483.
5 H. Gutte, A. E. Hansen, H. H. Johannesen, A. E. Clemmensen, J. H. Ardenkjær-Larsen, C. H. Nielsen and A. Kjær, The use of dynamic nuclear polarization $^{13}$C-pyruvate MRS in cancer, *Am. J. Nucl. Med. Mol. Imaging*, 2015, **5**, 548–560.
6 P. Nikolaou, B. M. Goodson and E. Y. Chekmenev, NMR Hyperpolarization Techniques for Biomedicine, *Chem.–Eur. J*, 2015, **21**, 3156–3166.
7 A. Comment, Dissolution DNP for *in vivo* preclinical studies, *J. Magn. Reson.*, 2016, **264**, 39–48.
8 J. H. Ardenkjaer-Larsen, B. Fridlund, A. Gram, G. Hansson, L. Hansson, M. H. Lerche, R. Servin, M. Thaning and K. Golman, Increase in signal-to-noise ratio of > 10,000 times in liquid-state NMR, *Proc. Natl. Acad. Sci.*, 2003, **100**, 10158–10163.
9 J. B. Hövener, A. N. Pravdivtsev, B. Kidd, C. R. Bowers, S. Glöggler, K. V. Kovtunov, M. Plaumann, R. Katz-Brull, K. Buckenmaier, A. Jerschow, F. Reineri, T. Theis, R. V. Shchepin, S. Wagner, P. Bhattacharya, N. M. Zacharias and E. Y. Chekmenev, Parahydrogen-Based Hyperpolarization for Biomedicine, *Angew. Chem., Int. Ed.*, 2018, **57**, 11140–11162.
10 S. Glöggler, J. Colell and S. Appelt, Para-hydrogen perspectives in hyperpolarized NMR, *J. Magn. Reson.*, 2013, **235**, 130–142.
11 S. B. Duckett and R. E. Mewis, Application of Parahydrogen Induced Polarization Techniques in NMR Spectroscopy and Imaging, *Acc. Chem. Res.*, 2012, **45**, 1247–1257.
12 R. W. Adams, J. A. Aguilar, K. D. Atkinson, M. J. Cowley, P. I. P. Elliott, S. B. Duckett, G. G. R. Green, I. G. Khazal, J. López-Serrano and D. C. Williamson, Reversible Interactions with para-Hydrogen Enhance NMR Sensitivity by Polarization Transfer, *Science*, 2009, **323**, 1708.
13 M. L. Truong, T. Theis, A. M. Coffey, R. V. Shchepin, K. W. Waddell, F. Shi, B. M. Goodson, W. S. Warren and E. Y. Chekmenev, $^{15}$N Hyperpolarization by Reversible Exchange Using SABRE-SHEATH, *J. Phys. Chem. C*, 2015, **119**, 8786–8797.
14 T. Theis, M. L. Truong, A. M. Coffey, R. V. Shchepin, K. W. Waddell, F. Shi, B. M. Goodson, W. S. Warren and E. Y. Chekmenev, Microtesla SABRE enables 10% nitrogen-15 nuclear spin polarization, *J. Am. Chem. Soc.*, 2015, **137**, 1404–1407.
15 K. V. Kovtunov, E. V. Pokochueva, O. G. Salnikov, S. F. Cousin, D. Kurzbach, B. Vuichoud, S. Jannin, E. Y. Chekmenev, B. M. Goodson, D. A. Barskiy and I. V. Koptyug, Hyperpolarized NMR Spectroscopy: d-DNP, PHIP, and SABRE Techniques, *Asian J. Chem.*, 2018, **13**, 1857–1871.
16 M. E. Halse, Perspectives for hyperpolarisation in compact NMR, *TrAC, Trends Anal. Chem.*, 2016, **83**, 76–83.
17 G. Zhang and C. Hilty, Applications of dissolution dynamic nuclear polarization in chemistry and biochemistry, *Magn. Reson. Chem.*, 2018, **56**, 566–582.
18 K. Chen and X. Chen, Design and development of molecular imaging probes, *Curr. Top. Med. Chem.*, 2010, **10**, 1227–1236.
19 R. Weissleder and U. Mahmood, Molecular imaging, *Radiology*, 2001, **219**, 316–333.
20 K. R. Keshari and D. M. Wilson, Chemistry and biochemistry of $^{13}$C hyperpolarized magnetic resonance using dynamic nuclear polarization, *Chem. Soc. Rev.*, 2014, **43**, 1627–1659.
21 Z. J. Wang, M. A. Ohliger, P. E. Z. Larson, J. W. Gordon, R. A. Bok, J. Slater, J. E. Villanueva-Meyer, C. P. Hess, J. Kurhanewicz and D. B. Vigneron, Hyperpolarized $^{13}$C MRI: State of the Art and Future Directions, *Radiology*, 2019, **291**, 273–284.
22 R. E. Hurd, Y. F. Yen, A. Chen and J. H. Ardenkjaer-Larsen, Hyperpolarized $^{13}$C metabolic imaging using dissolution dynamic nuclear polarization, *J. Magn. Reson. Imaging*, 2012, **36**, 1314–1328.
23 A. Comment and M. E. Merritt, Hyperpolarized Magnetic Resonance as a Sensitive Detector of Metabolic Function, *Biochem*, 2014, **53**, 7333–7357.
24 K. M. Brindle, Imaging Metabolism with Hyperpolarized $^{13}$C-Labeled Cell Substrates, *J. Am. Chem. Soc.*, 2015, **137**, 6418–6427.
25 J. Kurhanewicz, D. B. Vigneron, J. H. Ardenkjaer-Larsen, J. A. Bankson, K. Brindle, C. H. Cunningham, F. A. Gallagher, K. R. Keshari, A. Kjaer, C. Laustsen, D. A. Mankoff, M. E. Merritt, S. J. Nelson, J. M. Pauly, P. Lee, S. Ronen, D. J. Tyler, S. S. Rajan, D. M. Spielman, L. Wald, X. Zhang, C. R. Malloy and R. Rizi, Hyperpolarized $^{13}$C MRI: Path to Clinical Translation in Oncology, *Neoplasia*, 2019, **21**, 1–16.
26 Y. Kondo, H. Nonaka, Y. Takakusagi and S. Sando, Design of Nuclear Magnetic Resonance Molecular Probes for Hyperpolarized Bioimaging, *Angew. Chem., Int. Ed.*, 2021, **60**, 14779–14799.
27 R. L. Hesketh and K. M. Brindle, Magnetic resonance imaging of cancer metabolism with hyperpolarized $^{13}$C-labeled cell metabolites, *Curr. Opin. Chem. Biol.*, 2018, **45**, 187–194.
28 S. Meier, P. R. Jensen, M. Karlsson and M. H. Lerche, Hyperpolarized NMR Probes for Biological Assays, *Sensors*, 2014, **14**, 1576–1597.
29 M. Witanowski, Nitrogen nmr spectroscopy, *Pure Appl. Chem.*, 1974, **37**, 225–233.
30 N. V. Chukanov, R. V. Shchepin, S. M. Joshi, M. S. H. Kabir, O. G. Salnikov, A. Svyatova, I. V. Koptyug, J. G. Gelovani and E. Y. Chekmenev, Synthetic Approaches for $^{15}$N-Labeled Hyperpolarized Heterocyclic Molecular Imaging Agents for $^{15}$N NMR Signal Amplification by Reversible Exchange in

Microtesla Magnetic Fields, *Chem.–Eur. J.*, 2021, **27**, 9727–9736.

31 E. Ackerstaff, K. Glunde and Z. M. Bhujwalla, Choline phospholipid metabolism: A target in cancer cells, *J. Cell. Biochem.*, 2003, **90**, 525–533.

32 F. Podo, Tumour phospholipid metabolism, *NMR Biomed.*, 1999, **12**, 413–439.

33 C. Gabellieri, S. Reynolds, A. Lavie, G. S. Payne, M. O. Leach and T. R. Eykyn, Therapeutic Target Metabolism Observed Using Hyperpolarized $^{15}$N Choline, *J. Am. Chem. Soc.*, 2008, **130**, 4598–4599.

34 H. Allouche-Arnon, A. Gamliel, C. M. Barzilay, R. Nalbandian, J. M. Gomori, M. Karlsson, M. H. Lerche and R. Katz-Brull, A hyperpolarized choline molecular probe for monitoring acetylcholine synthesis, *Contrast Media Mol. Imaging*, 2011, **6**, 139–147.

35 C. Cudalbu, A. Comment, F. Kurdzesau, R. B. van Heeswijk, K. Uffmann, S. Jannin, V. Denisov, D. Kirik and R. Gruetter, Feasibility of *in vivo* $^{15}$N MRS detection of hyperpolarized $^{15}$N labeled choline in rats, *Phys. Chem. Chem. Phys.*, 2010, **12**, 5818–5823.

36 L. J. Friesen-Waldner, T. P. Wade, K. Thind, A. P. Chen, J. M. Gomori, J. Sosna, C. A. McKenzie and R. Katz-Brull, Hyperpolarized choline as an MR imaging molecular probe: Feasibility of *in vivo* imaging in a rat model, *J. Magn. Reson. Imaging*, 2015, **41**, 917–923.

37 R. Sarkar, A. Comment, P. R. Vasos, S. Jannin, R. Gruetter, G. Bodenhausen, H. Hall, D. Kirik and V. P. Denisov, Proton NMR of $^{15}$N-Choline Metabolites Enhanced by Dynamic Nuclear Polarization, *J. Am. Chem. Soc.*, 2009, **131**, 16014–16015.

38 K. Kumagai, K. Kawashima, M. Akakabe, M. Tsuda, T. Abe and M. Tsuda, Synthesis and hyperpolarized $^{15}$N NMR studies of $^{15}$N-choline-$d_{13}$, *Tetrahedron*, 2013, **69**, 3896–3900.

39 L. B. Bales, K. V. Kovtunov, D. A. Barskiy, R. V. Shchepin, A. M. Coffey, L. M. Kovtunova, A. V. Bukhtiyarov, M. A. Feldman, V. I. Bukhtiyarov, E. Y. Chekmenev, I. V. Koptyug and B. M. Goodson, Aqueous, Heterogeneous para-Hydrogen-Induced $^{15}$N Polarization, *J. Phys. Chem. C*, 2017, **121**, 15304–15309.

40 E. Chiavazza, A. Viale, M. Karlsson and S. Aime, $^{15}$N-Permethylated amino acids as efficient probes for MRI-DNP applications, *Contrast Media Mol. Imaging*, 2013, **8**, 417–421.

41 M. Durst, E. Chiavazza, A. Haase, S. Aime, M. Schwaiger and R. F. Schulte, alpha-trideuteromethyl[$^{15}$N]glutamine: A long-lived hyperpolarized perfusion marker, *Magn. Reson. Med.*, 2016, **76**, 1900–1904.

42 C. von Morze, J. A. Engelbach, G. D. Reed, A. P. Chen, J. D. Quirk, T. Blazey, R. Mahar, C. R. Malloy, J. R. Garbow and M. E. Merritt, $^{15}$N-carnitine, a novel endogenous hyperpolarized MRI probe with long signal lifetime, *Magn. Reson. Med.*, 2021, **85**, 1814–1820.

43 H. Mitsuya, K. J. Weinhold, P. A. Furman, M. H. St Clair, S. N. Lehrman, R. C. Gallo, D. Bolognesi, D. W. Barry and S. Broder, 3'-Azido-3'-deoxythymidine (BW A509U): an antiviral agent that inhibits the infectivity and cytopathic effect of human T-lymphotropic virus type III/lymphadenopathy-associated virus in vitro, *PNAS*, 1985, **82**, 7096–7100.

44 R. V. Shchepin and E. Y. Chekmenev, Toward hyperpolarized molecular imaging of HIV: synthesis and longitudinal relaxation properties of $^{15}$N-Azidothymidine, *J. Labelled Compd. Radiopharm.*, 2014, **57**, 621–624.

45 J. Bae, G. Zhang, H. Park, W. S. Warren and Q. Wang, $^{15}$N-Azides as practical and effective tags for developing long-lived hyperpolarized agents, *Chem. Sci.*, 2021, **12**, 14309–14315.

46 M. F. Murray, Nicotinamide: An Oral Antimicrobial Agent with Activity against Both Mycobacterium tuberculosis and Human Immunodeficiency Virus, *Clin. Infect. Dis.*, 2003, **36**, 453–460.

47 A. C. Chen, A. J. Martin, B. Choy, P. Fernández-Peñas, R. A. Dalziell, C. A. McKenzie, R. A. Scolyer, H. M. Dhillon, J. L. Vardy, A. Kricker, G. St. George, N. Chinniah, G. M. Halliday and D. L. Damian, A Phase 3 Randomized Trial of Nicotinamide for Skin-Cancer Chemoprevention, *N. Engl. J. Med.*, 2015, **373**, 1618–1626.

48 R. V. Shchepin, D. A. Barskiy, D. M. Mikhaylov and E. Y. Chekmenev, Efficient Synthesis of Nicotinamide-1-$^{15}$N for Ultrafast NMR Hyperpolarization Using Parahydrogen, *Bioconjugate Chem.*, 2016, **27**, 878–882.

49 J. Dunn and A. Blight, Dalfampridine: a brief review of its mechanism of action and efficacy as a treatment to improve walking in patients with multiple sclerosis, *Curr. Med. Res. Opin.*, 2011, **27**, 1415–1423.

50 N. V. Chukanov, O. G. Salnikov, I. A. Trofimov, M. S. H. Kabir, K. V. Kovtunov, I. V. Koptyug and E. Y. Chekmenev, Synthesis and $^{15}$N NMR Signal Amplification by Reversible Exchange of [$^{15}$N] Dalfampridine at Microtesla Magnetic Fields, *Chemphyschem*, 2021, **22**, 960–967.

51 A. Gamliel, S. Uppala, G. Sapir, T. Harris, A. Nardi-Schreiber, D. Shaul, J. Sosna, J. M. Gomori and R. Katz-Brull, Hyperpolarized [$^{15}$N]nitrate as a potential long lived hyperpolarized contrast agent for MRI, *J. Magn. Reson.*, 2019, **299**, 188–195.

52 I. F. Tannock and D. Rotin, Acid pH in Tumors and Its Potential for Therapeutic Exploitation, *Cancer Res.*, 1989, **49**, 4373.

53 F. A. Gallagher, M. I. Kettunen, S. E. Day, D.-E. Hu, J. H. Ardenkjær-Larsen, R. i. t. Zandt, P. R. Jensen, M. Karlsson, K. Golman, M. H. Lerche and K. M. Brindle, Magnetic resonance imaging of pH *in vivo* using hyperpolarized $^{13}$C-labelled bicarbonate, *Nature*, 2008, **453**, 940.

54 D. E. Korenchan, R. R. Flavell, C. Baligand, R. Sriram, K. Neumann, S. Sukumar, H. VanBrocklin, D. B. Vigneron, D. M. Wilson and J. Kurhanewicz, Dynamic nuclear polarization of biocompatible $^{13}$C-enriched carbonates for *in vivo* pH imaging, *Chem. Commun.*, 2016, **52**, 3030–3033.

55 W. Jiang, L. Lumata, W. Chen, S. Zhang, Z. Kovacs, A. D. Sherry and C. Khemtong, Hyperpolarized $^{15}$N-

pyridine Derivatives as pH-Sensitive MRI Agents, *Sci. Rep.*, 2015, **5**, 9104.

56 R. V. Shchepin, D. A. Barskiy, A. M. Coffey, T. Theis, F. Shi, W. S. Warren, B. M. Goodson and E. Y. Chekmenev, N-15 Hyperpolarization of Imidazole-N-15(2) for Magnetic Resonance pH Sensing *via* SABRE-SHEATH, *ACS Sens.*, 2016, **1**, 640–644.

57 B. E. Kidd, J. A. Mashni, M. N. Limbach, F. Shi, E. Y. Chekmenev, Y. Hou and B. M. Goodson, Toward Cleavable Metabolic/pH Sensing "Double Agents" Hyperpolarized by NMR Signal Amplification by Reversible Exchange, *Chem.–Eur. J.*, 2018, **24**, 10641–10645.

58 M. Fekete, F. Ahwal and S. B. Duckett, Remarkable Levels of $^{15}$N Polarization Delivered through SABRE into Unlabeled Pyridine, Pyrazine, or Metronidazole Enable Single Scan NMR Quantification at the mM Level, *J. Phys. Chem. B*, 2020, **124**, 4573–4580.

59 H. Nonaka, R. Hata, T. Doura, T. Nishihara, K. Kumagai, M. Akakabe, M. Tsuda, K. Ichikawa and S. Sando, A platform for designing hyperpolarized magnetic resonance chemical probes, *Nat. Commun.*, 2013, **4**, 2411.

60 W. R. Wilson and M. P. Hay, Targeting hypoxia in cancer therapy, *Nat. Rev. Cancer*, 2011, **11**, 393–410.

61 D. A. Barskiy, R. V. Shchepin, A. M. Coffey, T. Theis, W. S. Warren, B. M. Goodson and E. Y. Chekmenev, Over 20% $^{15}$N Hyperpolarization in Under One Minute for Metronidazole, an Antibiotic and Hypoxia Probe, *J. Am. Chem. Soc.*, 2016, **138**, 8080–8083.

62 R. V. Shchepin, J. R. Birchall, N. V. Chukanov, K. V. Kovtunov, I. V. Koptyug, T. Theis, W. S. Warren, J. G. Gelovani, B. M. Goodson, S. Shokouhi, M. S. Rosen, Y.-F. Yen, W. Pham and E. Y. Chekmenev, Hyperpolarizing Concentrated Metronidazole $^{15}NO_2$ Group over Six Chemical Bonds with More than 15% Polarization and a 20 Minute Lifetime, *Chem.–Eur. J.*, 2019, **25**, 8829–8836.

63 O. G. Salnikov, N. V. Chukanov, A. Svyatova, I. A. Trofimov, M. S. H. Kabir, J. G. Gelovani, K. V. Kovtunov, I. V. Koptyug and E. Y. Chekmenev, $^{15}$N NMR Hyperpolarization of Radiosensitizing Antibiotic Nimorazole by Reversible Parahydrogen Exchange in Microtesla Magnetic Fields, *Angew. Chem., Int. Ed.*, 2021, **60**, 2406–2413.

64 J. R. Birchall, M. S. H. Kabir, O. G. Salnikov, N. V. Chukanov, A. Svyatova, K. V. Kovtunov, I. V. Koptyug, J. G. Gelovani, B. M. Goodson, W. Pham and E. Y. Chekmenev, Quantifying the effects of quadrupolar sinks *via* $^{15}$N relaxation dynamics in metronidazoles hyperpolarized *via* SABRE-SHEATH, *Chem. Commun.*, 2020, **56**, 9098–9101.

65 H. P. Cheng, S. Wei, L. P. Wei and A. Verkhratsky, Calcium signaling in physiology and pathophysiology, *Acta Pharmacol. Sin.*, 2006, **27**, 767–772.

66 R. Hata, H. Nonaka, Y. Takakusagi, K. Ichikawa and S. Sando, Design of a hyperpolarized $^{15}$N NMR probe that induces a large chemical-shift change upon binding of calcium ions, *Chem. Commun.*, 2015, **51**, 12290–12292.

67 C. J. Frederickson, J.-Y. Koh and A. I. Bush, The neurobiology of zinc in health and disease, *Nat. Rev. Neurosci.*, 2005, **6**, 449–462.

68 L. De Leon-Rodriguez, A. J. M. Lubag and A. Dean Sherry, Imaging free zinc levels *in vivo* – What can be learned?, *Inorg. Chim. Acta*, 2012, **393**, 12–23.

69 E. H. Suh, J. M. Park, L. Lumata, A. D. Sherry and Z. Kovacs, Hyperpolarized $^{15}$N-labeled, deuterated tris(2-pyridylmethyl) amine as an MRI sensor of freely available $Zn^{2+}$, *Commun. Chem.*, 2020, **3**, 185.

70 T. Theis, G. X. Ortiz Jr, A. W. Logan, K. E. Claytor, Y. Feng, W. P. Huhn, V. Blum, S. J. Malcolmson, E. Y. Chekmenev, Q. Wang and W. S. Warren, Direct and cost-efficient hyperpolarization of long-lived nuclear spin states on universal $^{15}N_2$-diazirine molecular tags, *Sci. Adv.*, 2016, **2**, e1501438.

71 J. R. Hill and A. A. B. Robertson, Fishing for drug targets: a focus on diazirine photoaffinity probe synthesis, *J. Med. Chem.*, 2018, **61**, 6945–6963.

72 L. Dubinsky, B. P. Krom and M. M. Meijler, Diazirine based photoaffinity labeling, *Bioorg. Med. Chem.*, 2012, **20**, 554–570.

73 K. Shen, A. W. J. Logan, J. F. P. Colell, J. Bae, G. X. Ortiz Jr, T. Theis, W. S. Warren, S. J. Malcolmson and Q. Wang, Diazirines as potential molecular imaging tags: probing the requirements for efficient and long-lived SABRE-induced hyperpolarization, *Angew. Chem., Int. Ed.*, 2017, **56**, 12112–12116.

74 H. Park, G. Zhang, J. Bae, T. Theis, W. S. Warren and Q. Wang, Application of $^{15}N_2$-Diazirines as a Versatile Platform for Hyperpolarization of Biological Molecules by d-DNP, *Bioconjugate Chem.*, 2020, **31**, 537–541.

75 N. J. Agard, J. M. Baskin, J. A. Prescher, A. Lo and C. R. Bertozzi, A comparative study of bioorthogonal reactions with azides, *ACS Chem. Biol.*, 2006, **1**, 644–648.

76 S. Brase, C. Gil, K. Knepper and V. Zimmermann, Organic azides: An exploding diversity of a unique class of compounds, *Angew. Chem., Int. Ed.*, 2005, **44**, 5188–5240.